Generation of macroscopic singlet states in a cold atomic ensemble

N. Behbood,[1] F. Martin Ciurana,[1] G. Colangelo,[1] M. Napolitano,[1] G.Tóth,[2,3,4] R.J. Sewell,[1] and M.W. Mitchell[1,5]

[1] *ICFO-Institut de Ciencies Fotoniques, Mediterranean Technology Park, 08860 Castelldefels (Barcelona), Spain**

[2] *Department of Theoretical Physics, University of the Basque Country UPV/EHU, P.O. Box 644, E-48080 Bilbao, Spain*

[3] *IKERBASQUE, Basque Foundation for Science, E-48011 Bilbao, Spain*

[4] *Wigner Research Centre for Physics, Hungarian Academy of Sciences, P.O. Box 49, H-1525 Budapest, Hungary*

[5] *ICREA – Institució Catalana de Recerca i Estudis Avançats, 08015 Barcelona, Spain*

(Dated: March 11, 2014)

We report the generation of a macroscopic singlet state in a cold atomic sample via quantum non-demolition (QND) measurement induced spin squeezing. We observe 3 dB of spin squeezing and detect entanglement of up to 5.5×10^5 atoms with 5σ statistical significance using a generalized spin squeezing inequality. The degree of squeezing implies at least 50% of the atoms have formed singlets, while the response to a magnetic field gradient indicates entanglement bonds at all length scales, a characteristic of quantum spin liquids.

PACS numbers: 03.67.Bg,03.67.Mn,42.50.Dv

Some of the most striking phenomena in condensed matter physics, for example high-temperature superconductivity, are thought to result from large-scale spin entanglement. Shortly after the discovery of cuprate superconductors, Anderson proposed that a quantum spin liquid (QSL) [1], consisting of delocalized spin singlets induced by frustration in the anti-ferromagnetic (AF) system of Cu-bound electrons, was responsible for the extraordinarily high transition temperatures [2]. Such long-range entanglement has proven quite challenging to generate and study, both in natural condensed matter systems [3] and in quantum simulators [4, 5].

Here we report the production of large-scale and long-range singlet entanglement in an atomic system, using collective quantum non-demolition (QND) measurement [6, 7] as a global entanglement generator. The method, closely related to proposals using QND measurement to detect long-range correlations [8–11], first generates large-scale atom-light entanglement by passing a macroscopic optical pulse through the entire ensemble. The optical pulse is then measured, transferring the entanglement onto the atoms and leaving them in an entangled state [12]. Subsequent measurements on the ensemble confirm the presence of a macroscopic singlet state [13] with a singlet fraction of approximately one half. Conversion of the singlets to triplets with a magnetic field gradient confirms the presence of singlets at all length scales.

A macroscopic spin singlet has a collective spin $\hat{\mathbf{F}}=0$, where $\hat{\mathbf{F}}\equiv\sum_i\hat{\mathbf{f}}^{(i)}$ and $\hat{\mathbf{f}}^{(i)}$ the spin of the i'th atom. This implies that fluctuations in the collective spin vanish, i.e. $\boldsymbol{\Delta}\hat{\mathbf{F}}=0$, suggesting that we can both produce and detect a macroscopic singlet via QND measurement induced spin squeezing [11, 12]. Indeed, it has been shown that a macroscopic spin singlet can be detected via the generalized spin squeezing parameter

$$\xi^2=\frac{\sum_k(\Delta\hat{F}_k)^2}{fN_A} \tag{1}$$

where $\xi^2<1$ indicates spin squeezing and detects entanglement among the atoms [12, 14]. The standard quantum limit (SQL) for unpolarized atoms is set by $\xi^2=1$, i.e. $\sum_k(\Delta\hat{F}_k)^2=fN_A$. The number of atoms that are (pairwise) entangled in such a squeezed state is lower-bounded by $(1-\xi^2)N_A$ [12]. In the limit $\xi^2\to0$, the macroscopic many-body state is a true spin singlet.

Since the collective spin obeys spin uncertainty relations $(\Delta\hat{F}_i)^2(\Delta\hat{F}_j)^2\geq|\langle\hat{F}_k\rangle|^2/4$ (we take $\hbar=1$ throughout), squeezing all three spin components requires maintaining an unpolarized atomic sample with $\langle\hat{F}_k\rangle\simeq0$. Our experiment starts from a thermal spin state (TSS), i.e. a completely mixed state described by a density matrix $R=\rho^{\otimes N_A}$, where $\rho=\frac{1}{3}\mathbb{1}_{3\times3}$ and $\mathbb{1}_{3\times3}$ is the identity matrix. This state is symmetric under exchange of atoms, and mixed at the level of each atom. We probe the atoms with pulses of near-resonant light described by Stokes operators $\boldsymbol{S}$ describing the light polarization, which obey $[\hat{S}_\mathrm{x},\hat{S}_\mathrm{y}]=i\hat{S}_\mathrm{z}$ and cyclic permutations. The input pulses are fully $\hat{S}_\mathrm{x}$-polarized, i.e. with $\langle\hat{S}_\mathrm{x}\rangle=N_\mathrm{L}/2$, where N_L is the number of photons in the pulse. During a measurement pulse, the atoms and light interact via an effective hamiltonian (see Supplementary material)

$$\tau\hat{H}_\mathrm{eff}=G_1\hat{S}_\mathrm{z}\hat{F}_\mathrm{z} \tag{2}$$

where G_1 is a coupling constant describing the vector lights shift and τ is the pulse duration [15, 16]. Eq. (2) describes a QND measurement of $\hat{F}_\mathrm{z}$, i.e., a measurement with no back-action on $\hat{F}_\mathrm{z}$. We detect the output

$$\hat{S}_\mathrm{y}^{(\mathrm{out})}=\hat{S}_\mathrm{y}^{(\mathrm{in})}+G_1\hat{S}_\mathrm{x}^{(\mathrm{in})}\hat{F}_\mathrm{z}^{(\mathrm{in})} \tag{3}$$

which leads to measurement-induced conditional spin squeezing of the $\hat{F}_\mathrm{z}$ component by a factor $1/(1+\zeta)$,

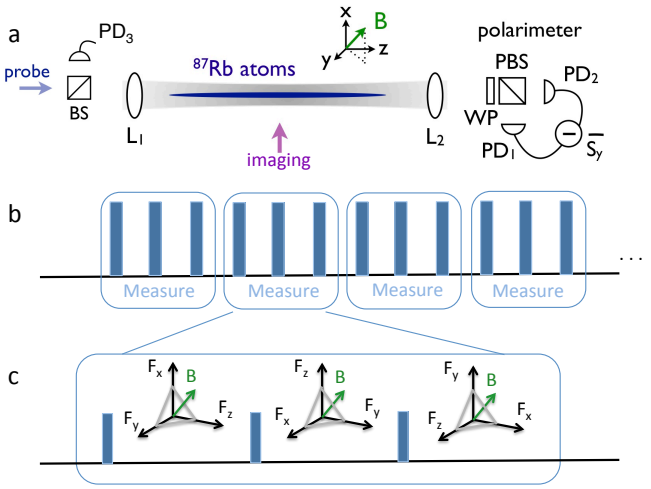

FIG. 1. (Color online) (a) Experimental geometry. Near-resonant probe pulses pass through a cold cloud of ^{87}Rb atoms and experience a Faraday rotation by an angle proportional to the on-axis collective spin $\hat{F}_z$. The pulses are initially polarized with maximal Stokes operator $\hat{S}_x$ recorded on reference detector (PD3). Rotation toward $\hat{S}_y$ is detected by a balanced polarimeter consisting of a wave plate (WP), polarizing beam splitter (PBS), and photodiodes (PD1,2). $\hat{\mathbf{F}}$ precesses about a magnetic field ($\mathbf{B}$) along the direction [111] making all components accessible to measure through stroboscopic probing. (b),(c) Pulse sequence: A first QND measurement measures the $\hat{F}_z$ angular momentum component and the second and third QND measurements in 1/3 and 2/3 of Larmor precession cycles are measuring $\hat{F}_y$ and $\hat{F}_x$ respectively.

where $\zeta = \frac{2}{3}G_1^2 N_L N_A$ is the signal-to-noise ratio (SNR) of the measurement [17].

To measure and squeeze the remaining spin components, we follow a stroboscopic probing strategy described in Refs. [18, 19]. We apply a magnetic field along the [1,1,1] direction so that the collective atomic spin rotates $\hat{F}_z \to \hat{F}_x \to \hat{F}_y$ during one Larmor precession cycle. We then time our probe pulses to probe the atoms at $T_L/3$ intervals, allowing us to measure all three components of the collective spin in one Larmor period. Note that the probe duration $\tau \ll T_L$, so that we can neglect the rotation of the atomic spin during a probe pulse.

This measurement procedure respects the exchange symmetry of the input TSS, and generates correlations among pairs of atoms independent of the distance between them, leading to non-local and long-range entanglement of the atomic spins. The resulting state resembles a high-temperature spin liquid with $(1-\xi^2)N_A$ spins entangled in a macroscopic singlet state, and $\xi^2 N_A$ spin excitations (spinons).

Our experimental apparatus, illustrated in Fig. 1(a), is described in detail in Refs. [20]. In each cycle of the experiment we trap up to 1.5×10^6 ^{87}Rb atoms in a weakly focused single beam optical dipole trap. The atoms are laser-cooled to a temperature of 20 μK, and optically

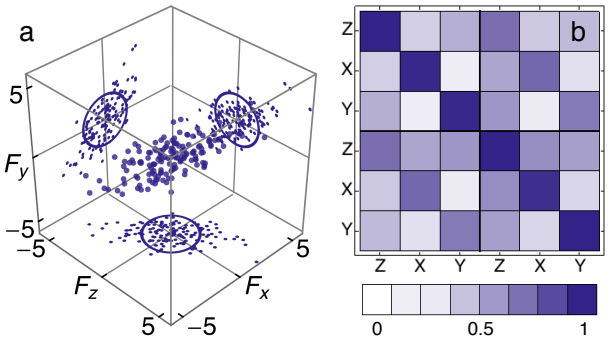

FIG. 2. (Color online) Measured spin distribution (a) of the input TSS following the state preparation procedure described in the main text, and correlation matrix (b) between two consecutive three-component collective spin measurements showing strong correlations between measurements of each spin component $\hat{F}_i$. For presentation purposes an offset has been subtracted from the data in (a).

pumped into the $f = 1$ hyperfine ground state. We probe the atoms via paramagnetic Faraday rotation using pulses of near-resonant propagating along the trap axis to give a high-sensitivity measurement of $\hat{F}_z$. A shot-noise-limited balanced polarimeter detects $\hat{S}_y^{(\mathrm{out})}$ while a reference detector before the atoms measures $\hat{S}_x^{(\mathrm{in})}$. The trap geometry produces a large atom-light interaction for light pulses propagating along the axis of the trap, quantified by the effective optical depth $d_0 = (\sigma_0/A)N_A$, where $\sigma_0 = \lambda^2/\pi$ and $A = 2.7\times10^{-9}$ m is the effective atom-light interaction area [20], giving $d_0 = 69.5$ with $N_A = 1.5\times10^6$ atoms. We measure an atom-light coupling constant $G_1 = 9.0\pm0.1\times10^{-8}$ radians per spin (see Supplementary material). The measured sensitivity of the Faraday rotation probing is $\Delta F_z = 515$ spins, allowing projection-noise-limited probing of an input TSS with $N_A > 1.75\times10^5$ atoms.

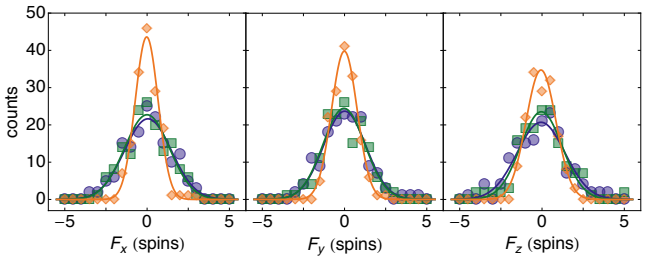

FIG. 3. Individual spin measurements. Histograms of the measurements of each of the three spin components in the first round (blue circles) and second round (green squares) of the stroboscopic probe. We also show the conditional spin distribution $F_k^{(2)} - \chi F_k^{(1)}$ (orange diamonds), where $\chi \equiv \mathrm{cov}(F_k^{(1)}, F_k^{(2)})/(\Delta F_k^{(1)})^2$ is the degree of correlation. For presentation purposes an offset has been subtracted from the data.

The measurement sequence is illustrated in Figs. 1(b),(c). For each measurement, the atoms are initially prepared in a TSS via repeated optical pumping of the atoms between $f = 1$ and $f = 2$, as described in Ref. [6]. We then probe the atomic spins using a train of $\tau = 1$ μs long pulses of linearly polarized light, detuned by 700 MHz to red of the $f = 1 \rightarrow f' = 0$ transition of the D_2 line. Each pulse contains on average $N_L = 2.8 \times 10^8$ photons. To access also $\hat{F}_x$ and $\hat{F}_y$, we apply a magnetic field with a magnitude $B = 15.9 \pm 0.1$ mG along the direction [111]. The atomic spins precess around this applied field with a Larmor period of $T_L = 90$ μs $\gg \tau$, and we probe the atoms at $T_L/3 = 30$ μs intervals for five Larmor periods, allowing us to analyze the statistics of repeated QND measurements of the collective spin.

After the QND probing, the number of atoms N_A is quantified via dispersive atom number measurement (DANM) [6] by applying a bias field $B_z = 100$ mG and optically pumping the atoms into $|f = 1, m_f = 1\rangle$ with circularly-polarized light propagating along the trap axis resonant with the $f = 1 \rightarrow f' = 1$ transition, and then probing with the Faraday rotation probe.

The sequence of state-preparation, stroboscopic probing and DANM is repeated 12 times per trap loading cycle. In each sequence $\sim 15\%$ of the atoms are lost, mainly during the state-preparation, so that different values of N_A are sampled during each loading cycle. At the end of each cycle the measurement is repeated without atoms in the trap. The loading cycle is repeated 155 times to collect statistics.

In Fig. 2(a) we plot the spin distribution $\mathbf{F}^{(1)}$ of the collective spin of a sample with $N_A = 1.4 \times 10^6$ atoms measured by the first three probe pulses. We measure an initial spin covariance matrix of

$$\Gamma_1 = \begin{pmatrix} 1.90 & 1.10 & 1.10 \\ 1.10 & 1.40 & 0.81 \\ 1.10 & 0.81 & 1.30 \end{pmatrix} \times 10^6 \,\mathrm{spins}^2 \qquad (4)$$

where $(\Gamma_c)_{ij} \equiv \mathrm{cov}(\hat{F}_i^{(c)}, \hat{F}_j^{(c)}) \equiv \frac{1}{2}\langle \hat{F}_i^{(c)}\hat{F}_j^{(c)} + \hat{F}_j^{(c)}\hat{F}_i^{(c)}\rangle - \langle \hat{F}_i^{(c)}\rangle\langle \hat{F}_j^{(c)}\rangle$. For comparison, an ideal TSS would have $\Gamma = \mathrm{diag}(0.93, 0.93, 0.93) \times 10^6$ spins^2 with the same number of atoms. The larger measured variances, and non-zero covariances, in Γ_1 indicate the presence of atomic technical noise due to imperfect state preparation and shot-to-shot fluctuations in the atom number and applied magnetic field.

In Fig. 2(b) we plot the correlations $\mathrm{cov}(\hat{F}_i, \hat{F}_j)/\Delta\hat{F}_i\Delta\hat{F}_j$ between the first six QND measurements. The off-diagonal elements indicate that successive measurements of the same spin component $\hat{F}_k$ are correlated. This allows us to predict the outcome of the second measurements $F_k^{(2)}$ with a reduced conditional uncertainty. For a single parameter, the conditional variance is $\mathrm{var}(F_k^{(2)}|F_k^{(1)}) \equiv \mathrm{var}(F_k^{(2)} - \chi F_k^{(2)})$, where

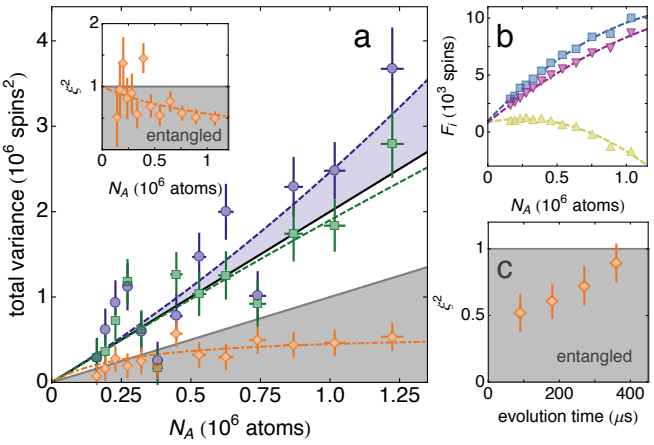

FIG. 4. (Color online) (a) Noise scaling of total variance of the first (blue circles) and second (green squares) QND measurement of the atomic spin distribution. Dashed lines are a quadratic fit, indicating the presence of technical noise in the input atomic state (blue shaded region). Black line indicates the expected quantum noise $\widetilde{\mathcal{V}} = 2N_A$ due to an ideal TSS. Shaded area represents region with $\widetilde{\mathcal{V}}_{2|1} < fN_A$, indicating spin squeezing and entanglement. Orange dot-dashed curve is a fit to the expected conditional noise reduction with the SNR of the QND measurement as a free parameter. Inset: Semi-log plot of detected spin squeezing parameter. Dot-dashed curve is a the expected spin squeezing calculated from the fitted SNR. (b) Measured average spin components $\langle \hat{F}_k \rangle$. (c) Spin squeezing as a function of hold time. We plot the conditional variance $\widetilde{\mathcal{V}}_{p|1}$, where $p = \{2, 3, 4, 5\}$, between the first and subsequent four QND measurements, made at $T_L = 90.1$ μs intervals. Entanglement is detected with 1σ significance after 360 μs. In all figures horizontal and vertical error bars represent 1σ statistical errors. In (a) and (c) read-out noise has been subtracted from the data.

the correlation parameter $\chi \equiv \mathrm{cov}(F_k^{(1)}, F_k^{(2)})/\mathrm{var}(F_k^{(1)})$ minimizes the conditional variance [21]. This is illustrated in Fig. 3. The residual correlation between measurements of different spin components is due to correlated technical noise in the atomic state preparation, and in the detection system.

To quantify spin squeezing we calculate the total variance $\mathcal{V}_p \equiv \mathrm{Tr}(\Gamma_p)$ of the QND measurements. Conditional noise reduction is quantified via $\mathcal{V}_{2|1} = \mathrm{Tr}(\Gamma_{2|1})$, i.e. the total variance of the conditional covariance matrix $\Gamma_{2|1} \equiv \Gamma_2 - \Gamma_{2,1}\Gamma_1^{-1}\Gamma_{1,2}$ where $\Gamma_{1,2} \equiv \mathrm{cov}(\hat{F}_i^{(1)}, \hat{F}_j^{(2)})$ [22]. To estimate the atomic noise contribution we fit the polynomial $\mathcal{V}(N_A) = \mathcal{V}_0 + 2N_A + cN_A^2$ to the measured data, and calculate $\widetilde{\mathcal{V}}_p = \mathcal{V}_p - \mathcal{V}_0$, subtracting the read-out noise $\mathcal{V}_0$ from the measured total variances (see Supplementary material).

In Fig. 4(a) we plot $\widetilde{\mathcal{V}}(N_A)$ for the first two QND measurements (blue circles and green squares). An ideal TSS has $\widetilde{\mathcal{V}} = 2N_A$ (black line in Fig. 4(a)). The technical noise contribution to $\widetilde{\mathcal{V}}_1$ is indicated by the blue shaded region.

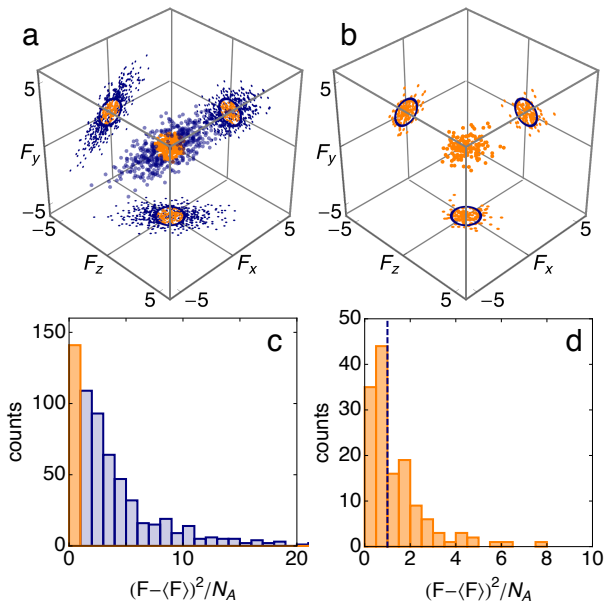

FIG. 5. (Color online) Selection of a macroscopic spin singlet. From the initial spin distribution (blue data in figure (a)), we select data with $|\hat{\mathbf{F}}^{(1)} - \langle\hat{\mathbf{F}}^{(1)}\rangle|^2/N_A < C$ (orange data in figure (a)), where C is a chosen cutoff parameter. We then analyze the second QND measurement $\hat{\mathbf{F}}^{(2)}$ of the same data (orange data in figure (b)) to detect spin squeezing and entanglement. We illustrate this with data from a sample with $N_A = 1.1 \times 10^6$ atoms and $C = 1$. Solid blue circles (a) and (b) have a radius $\sqrt{CN_A}$. In (c) and (d) we plot a histogram of the first and second measurements. The selected data are plotted in orange, and the dashed blue line in (d) indicates the cutoff.

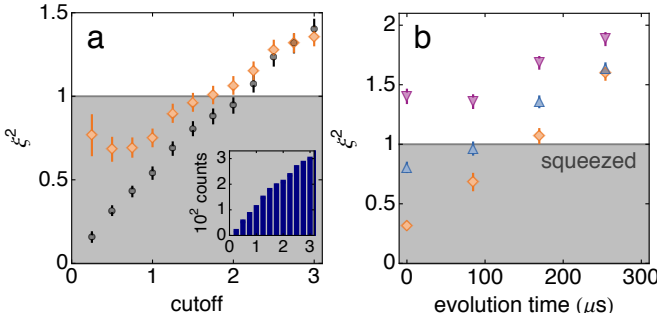

FIG. 6. (Color online) (a) Spin squeezing parameter ξ^2 (orange diamonds) calculated from the second QND measurement of the selected data as a function of the cutoff parameter C. For reference, the same parameter calculated from the first QND measurement is also plotted (black circles). Inset: number of selected data points included as a function of the cutoff parameter. (b) Spin squeezing as a function of evolution time in the trap, and initial squeezing. Data is shown for $C = 0.5$ (orange diamonds), 1.5 (blue triangles) and 3 (purple inverted triangles). Error bars indicate 1σ statistical errors.

A conditional variance $\widetilde{\mathcal{V}}_{2|1} < fN_A$ (shaded region) indicates spin squeezing and detects entanglement among the atoms [12, 14]. The measured conditional variance $\widetilde{\mathcal{V}}_{2|1}$ (orange diamonds) indicates we produce spin squeezed states for $N_A > 5 \times 10^5$ atoms. The conditional noise for an ideal QND measurement is $\widetilde{\mathcal{V}}_{2|1} = 2N_A/(1+\zeta)$, where $\zeta = \frac{2}{3}G_1^2 N_L N_A$ is the signal-to-noise ratio (SNR) of the measurement [17, 21]. A fit to our data (orange dot-dashed line) gives $\widetilde{\mathcal{V}}_{2|1} = 2N_A/(1+b\zeta)$ with $b = 0.75 \pm 0.1$, where the reduction in SNR is due to technical noise in the detection system. In the inset of Fig. 4(a) we show the calculated spin squeezing parameter $\xi^2 = \widetilde{\mathcal{V}}_{2|1}/fN_A$. With $N_A = 1.1 \times 10^6$ atoms we measure $\xi^2 = 0.50 \pm 0.09$, or 3dB of spin squeezing detected with 5σ significance, indicating that at minimum 5.5×10^5 atoms are entangled in the atomic sample [12], with a lifetime of over 300 μs (see Fig. 4(c)).

We observe a small residual atomic polarization due to atoms that are not entangled in the mascroscopic singlet state. In Fig. 4(b) we plot the mean spin components $\langle\hat{F}_k\rangle$ measured in the experiment. We observe a maximum $\langle F_k\rangle = 10.0 \pm 0.2 \times 10^3$ and $|F| = 13.3 \pm 0.3 \times 10^3$ spins with $N_A = 1.1 \times 10^6$ atoms. In principle with these values we could achieve 20dB of spin squeezing, entangling up to 99% of the atoms in a macroscopic singlet, before back-action due to the spin uncertainty relations limits the achievable squeezing. This residual polarization could be removed by adding a feedback loop to the measurement sequence as described in Ref. [19], which would produce an unconditionally squeezed macroscopic singlet centered at the origin.

To study the macroscopic singlet state in more detail, we repeated the experiment under similar conditions with a larger number (602) of repetitions of the trap loading cycle. This allows us to select from our data, with good statistical sensitivity, macroscopic spin singlets with varying amounts of squeezing produced under otherwise identical conditions. For these measurements the applied magnetic field had a magnitude $B = 16.9$ mG, giving a Larmor period of $T_L = 85 \pm 3$ μs.

The selection procedure is illustrated in Fig. 5. We select data from the first QND measurement using the criterion $|\hat{\mathbf{F}} - \langle\hat{\mathbf{F}}\rangle|^2/N_A < C$, where C is a chosen cutoff parameter. We then calculate $\xi^2 = \widetilde{\mathcal{V}}/(fN_A)$ from the second QND measurement of the selected preparations, where $\widetilde{\mathcal{V}}_2 = \mathcal{V} - \mathcal{V}_0$, $\mathcal{V} = \mathrm{Tr}(\Gamma_2)$ and $\mathcal{V}_0$ is measured without atoms in the trap. In Fig. 6(a) we show ξ^2 as a function of the cutoff parameter C for data from a sample with $N_A = 1.1 \times 10^6$ With a cutoff $C = 0.75$ we measure $\xi^2 = 0.69 \pm 0.05$, detecting entanglement with 5σ significance.

The singlet states that we prepare via this method contain long-range atomic entanglement due to the collective nature of the atom-light interaction. Atoms entangled in spin singlets are invariant under SU(2) rotations describing the effect of a homogeneous magnetic field, but

a gradient magnetic field can induce singlet-triplet spin flips, leading to decoherence of the macroscopic singlet. The rate at which this occurs depends on the average separation between entangled atoms in the sample.

Although the singlet is invariant under rotations due to homogeneous magnetic fields, we expect it to decohere in the presence of a *gradient magnetic* field, which will drive to singlet→triplet spin flips. In Fig. 6(b) we plot the evolution of singlet states with differing amounts of initial squeezing. The data points come from the second, third, forth and fifth QND measurement of the selected preparations, made at 84.7 μs intervals. As described in Ref. [13], for a Gaussian-distributed atomic sample this leads to an increase in measured spin noise at a rate $\xi(t) \propto \exp(-t^2/T_2^2)$, where $T_2 = 1/(\sigma\gamma\partial B/\partial z) = 809 \pm 30$ μs is the independently measured transverse coherence time(see Supplementary material) [18], γ is the atomic gyromagnetic ratio, $\sigma = 2.68 \pm 0.3$ mm the RMS width of the sample, and $\partial B/\partial z$ the gradient of the applied magnetic field. In contrast, the noise $\xi^2 = 2$ from a TSS does not change under the influence of a gradient field, and for a state with larger input noise, $\xi(t)$ will decrease towards $\xi^2 = 2$. The observed increase in $\xi(t)$ is further evidence for the presence of long-range entanglement in the macroscopic singlet state.

We have demonstrated the conditional preparation of a macroscopic singlet state via stroboscopic QND measurement. We observe 3dB of spin squeezing and detect entanglement of up to 5.5×10^5 atoms with 5σ statistical significance using a generalized spin squeezing inequality [12, 14]. Decoherence of the state is well described by a simple model, limited by magnetic field gradients, indicating the presence of atomic entanglement at many length scales, characteristic of a quantum spin liquid. Our techniques complement existing experimental methods [4, 5, 23, 24] and can be readily adapted to measurements of quantum lattice gases [8, 10, 11] and spinor condensates [9].

This work was supported by the Spanish MINECO (projects FIS2011-23520 and FIS2012-36673-C03-03), by the EU (projects ERC StG AQUMET, ERC StG GEDENTQOPT and CHIST-ERA QUASAR), by the Basque Government (Project No. IT4720-10), and by the OTKA (Contract No. K83858).

* naeimeh.behbood@icfo.es

[1] P. Anderson, Materials Research Bulletin, **8**, 153 (1973), ISSN 0025-5408.
[2] P. W. Anderson, Science, **235**, 1196 (1987).
[3] L. Balents, Nature, **464**, 199 (2010).
[4] S. Trotzky, Y.-A. Chen, U. Schnorrberger, P. Cheinet, and I. Bloch, Phys. Rev. Lett., **105**, 265303 (2010).
[5] J. Simon, W. S. Bakr, R. Ma, M. E. Tai, P. M. Preiss, and M. Greiner, Nature, **472**, 307 (2011).
[6] M. Koschorreck, M. Napolitano, B. Dubost, and M. W. Mitchell, Phys. Rev. Lett., **104**, 093602 (2010).
[7] R. J. Sewell, M. Napolitano, N. Behbood, G. Colangelo, and M. W. Mitchell, Nat. Photon., **7**, 517 (2013).
[8] K. Eckert, O. Romero-Isart, M. Rodriguez, M. Lewenstein, E. S. Polzik, and A. Sanpera, Nat. Phys., **4**, 50 (2008).
[9] K. Eckert, L. Zawitkowski, A. Sanpera, M. Lewenstein, and E. S. Polzik, Phys. Rev. Lett., **98**, 100404 (2007).
[10] K. G. L. Pedersen, B. M. Andersen, G. M. Bruun, O. F. Syljuåsen, and A. S. Sørensen, Phys. Rev. A, **84**, 041603 (2011).
[11] P. Hauke, R. J. Sewell, M. W. Mitchell, and M. Lewenstein, Phys. Rev. A, **87**, 021601 (2013).
[12] G. Tóth and M. W. Mitchell, New J. Phys., **12**, 053007 (2010).
[13] I. Urizar-Lanz, P. Hyllus, I. L. Egusquiza, M. W. Mitchell, and G. Tóth, Phys. Rev. A, **88**, 013626 (2013).
[14] G. Vitagliano, P. Hyllus, I. n. L. Egusquiza, and G. Tóth, Phys. Rev. Lett., **107**, 240502 (2011).
[15] S. R. de Echaniz, M. Koschorreck, M. Napolitano, M. Kubasik, and M. W. Mitchell, Phys. Rev. A, **77**, 032316 (2008).
[16] G. Colangelo, R. J. Sewell, N. Behbood, F. M. Ciurana, G. Triginer, and M. W. Mitchell, New J. Phys., **15**, 103007 (2013).
[17] K. Hammerer, K. Mølmer, E. S. Polzik, and J. I. Cirac, Phys. Rev. A, **70**, 044304 (2004).
[18] N. Behbood, F. M. Ciurana, G. Colangelo, M. Napolitano, M. W. Mitchell, and R. J. Sewell, Appl. Phys. Lett., **102**, 173504 (2013).
[19] N. Behbood, G. Colangelo, F. Martin Ciurana, M. Napolitano, R. J. Sewell, and M. W. Mitchell, Phys. Rev. Lett., **111**, 103601 (2013).
[20] M. Kubasik, M. Koschorreck, M. Napolitano, S. R. de Echaniz, H. Crepaz, J. Eschner, E. S. Polzik, and M. W. Mitchell, Phys. Rev. A, **79**, 043815 (2009).
[21] R. J. Sewell, M. Koschorreck, M. Napolitano, B. Dubost, N. Behbood, and M. W. Mitchell, Phys. Rev. Lett., **109**, 253605 (2012).
[22] M. Kendall and A. Stuart, *The advanced theory of statistics. Vol.2* (London, Griffin, 1979).
[23] D. Greif, L. Tarruell, T. Uehlinger, R. Jördens, and T. Esslinger, Phys. Rev. Lett., **106**, 145302 (2011).
[24] D. Greif, T. Uehlinger, G. Jotzu, L. Tarruell, and T. Esslinger, Science, **340**, 1307 (2013).

SUPPLEMENTARY MATERIAL

Atom-light interaction

We define the collective spin operator $\hat{\mathbf{F}} \equiv \sum_i \hat{\mathbf{f}}^{(i)}$, where $\hat{\mathbf{f}}^{(i)}$ is the spin of the i'th atom. The collective spin obeys commutation relations $[\hat{F}_\mathrm{x}, \hat{F}_\mathrm{y}] = i\hat{F}_\mathrm{z}$ (we take $\hbar = 1$ throughout). Probe pulses are described by the Stokes operator $\boldsymbol{S}$ defined as $\hat{S}_i \equiv \frac{1}{2}(\hat{a}_+^\dagger, \hat{a}_-^\dagger)\sigma_i(\hat{a}_+, \hat{a}_-)^T$, where the σ_i are the Pauli matrices and $\hat{a}_\pm$ are annihilation operators for $\sigma_\pm$ polarization, which obey $[\hat{S}_\mathrm{x}, \hat{S}_\mathrm{y}] = i\hat{S}_\mathrm{z}$ and cyclic permutations. The input pulses are fully $\hat{S}_\mathrm{x}$-polarized, i.e. with $\langle\hat{S}_\mathrm{x}\rangle = N_\mathrm{L}/2$, $\langle\hat{S}_\mathrm{y}\rangle = \langle\hat{S}_\mathrm{z}\rangle = 0$ and $\Delta^2 S_i = N_\mathrm{L}/4$, $i \in \{x, y, z\}$ where N_L is the number of photons in the pulse.

The atoms and light interact via an effective hamiltonian

$$\tau\hat{H}_\mathrm{eff} = G_1\hat{S}_\mathrm{z}\hat{F}_\mathrm{z} + G_2(\hat{S}_\mathrm{x}\hat{J}_\mathrm{x} + \hat{S}_\mathrm{y}\hat{J}_\mathrm{y} + \hat{S}_0\hat{J}_m/\sqrt{3}) \tag{5}$$

where G_1 and G_2 are coupling constants describing vector and tensor lights shifts, respectively, and τ is the pulse duration [15, 16]. The operators $\hat{J}_k \equiv \sum_i^{N_A} \hat{\jmath}_i$ where $\hat{\jmath}_x \equiv \hat{f}_x^2 - \hat{f}_y^2$ and $\hat{\jmath}_y \equiv \hat{f}_x\hat{f}_y + \hat{f}_y\hat{f}_x$ describe single-atom Raman coherences, i.e., coherences between states with m_f different by 2, and $\hat{\jmath}_m \equiv (3\hat{f}_z^2 - \hat{\mathbf{f}}^2)/\sqrt{3}$ describes the population difference between the $m_f = 0$ and $m_f = \pm 1$ magnetic sublevels.

The first term in Eq. (5) describes paramagnetic Faraday rotation: it rotates the polarization in the $\hat{S}_\mathrm{x}$, $\hat{S}_\mathrm{y}$ plane by an angle $\phi = G_1\hat{F}_\mathrm{z} \ll 1$, and leaves the atomic state unchanged, so that a measurement of $\hat{S}_\mathrm{y}^{(\mathrm{out})}/\hat{S}_\mathrm{x}^{(\mathrm{in})}$ indicates $\hat{F}_\mathrm{z}$ with a shot-noise-limited sensitivity of $\Delta\hat{F}_\mathrm{z} = \Delta\hat{S}_\mathrm{y}/G_1$. Acting alone, this describes a QND measurement of $\hat{F}_\mathrm{z}$, i.e., with no back-action on $\hat{F}_\mathrm{z}$. The second term, in contrast, leads to an optical rotation $\hat{S}_\mathrm{x} \to \hat{S}_\mathrm{z}$ (due to the birefringence of the atomic sample), and drives a rotation of the atomic spins in the $\hat{F}_\mathrm{z}$, $\hat{J}_y$ plane (alignment-to-orientation conversion) by an angle $\tan\theta = G_2\hat{S}_\mathrm{x}/2$ [16, 21]. This leads to a detected output

$$\hat{S}_\mathrm{y}^{(\mathrm{out})} = \hat{S}_\mathrm{y}^{(\mathrm{in})} + G_1\hat{S}_\mathrm{x}^{(\mathrm{in})}(\hat{F}_\mathrm{z}^{(\mathrm{in})} + \sin\theta\,\hat{J}_\mathrm{y}^{(\mathrm{in})}). \tag{6}$$

For the experiments described here $\theta \simeq 0.3$, and the $\sin\theta$ term can be safely ignored. The contribution of the remaining terms in Eq. (5) is negligible.

Atom-field interaction

The atoms interact with the applied magnetic field via the hamiltonian

$$\hat{H}_\mathrm{mag} = -\gamma\hat{\mathbf{F}}\cdot\mathbf{B}. \tag{7}$$

During a single probe-pulse the atomic spins rotate by an angle $\Theta = \gamma B\tau$, where $B = |\mathbf{B}|$. For our parameters $\Theta \simeq 0.01$ radians, so we can neglect the rotation of the spins during the probe pulses.

Probe calibration

The light-atom coupling constant G_1 is calibrated by correlating the DANM signal with an independent count of the atom number via absorption imaging [6, 20, 21]. In Fig. 7(a) we show the calibration data. We find $G_1 = 9.0\pm0.1\times10^{-8}$ radians per spin at the detuning $\Delta = -700$ MHz. In the inset of Fig. 7(a) we plot G_1 vs. Δ. We fit this data to find the effective atom-light interaction area A [20], from which we estimate the tensor light shift $G_2 = -4.1^{+0.4}_{-0.5} \times 10^{-9}$ radians per spin at $\Delta = -700$ MHz.

Magnetic field measurements

We measure the applied magnetic field using the atoms as an in-situ vector magnetometer. Our technique is described in detail in Ref. [18]. We polarize the atoms via optically pumping along first $\hat{F}_\mathrm{z}$ and then $\hat{F}_\mathrm{y}$, and observe the free induction decay (FID) of the resulting Larmor precession using the Faraday rotation probe. We model density

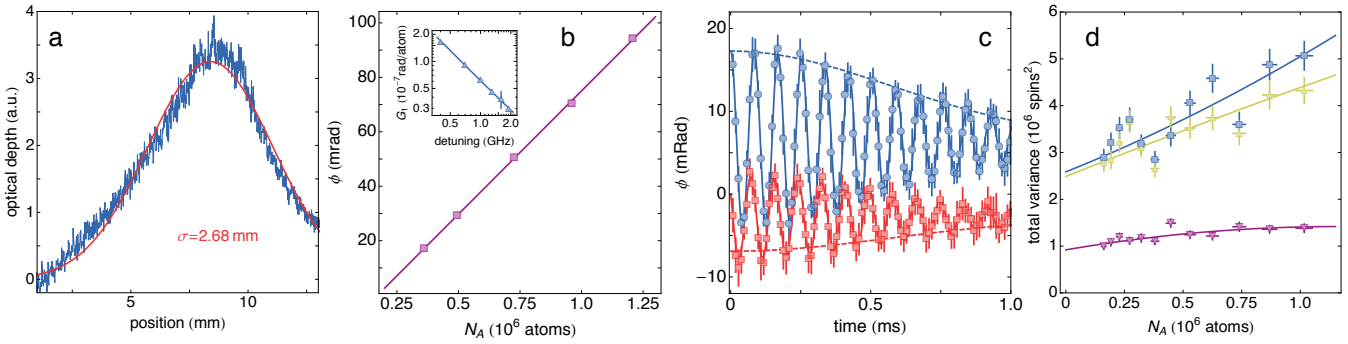

FIG. 7. (Color online) (a) The atomic density distribution, integrated over the radial direction, with a gaussian fit (red line), giving an RMS width $\sigma = 2.68 \pm 0.3$ mm. (b) Calibration of G_1 coupling constant. We correlate the observed rotation angle ϕ against an independent measurement of atom number N_A via absorption imaging. Inset: from a fit to G_1 vs. the probe detuning Δ we estimate the effective atom-light interaction area A and tensor light shift G_2. (c) Free induction decay (FID) measurement of the applied magnetic field using atoms as an in-situ vector magnetometer. Blue circles: input $\hat{F}_z$-polarized atomic state. Blue circles: input $\hat{F}_y$-polarized atomic state. Solid line: fit described by Eq. (8). Dashed line: gaussian envelope of FID signal. (d) Noise scaling of total variance $\mathcal{V}_p = \mathrm{Tr}(\Gamma_p)$ of the first two QND measurements, and conditional variance $\mathcal{V}_{2|1} = \mathrm{Tr}(\Gamma_{2|1})$. Blue squares: first measurement. Yellow triangles: second measurement. Purple inverted triangles: conditional variance.

distribution along the length of the trap with a gaussian $A\exp(-(z-z_0)^2/2\sigma^2)$, with an RMS width $\sigma = 2.68 \pm 0.3$ mm. A typical density profile and gaussian fit is shown in Fig. 7(a). This leads to observed signals for the two input states

$$\theta(t) = \frac{G_1}{B^2}\begin{cases} \left(B_z^2 + \left(B_x^2 + B_y^2\right)\cos\omega \exp\left(-t^2/T_2^2\right)\right) F_z(0) \\ \left(B_y B_z \left(1 - \cos\omega \exp\left(-t^2/T_2^2\right)\right) + B_x B \sin\omega \exp\left(-t^2/T_2^2\right)\right) F_y(0) \end{cases} \tag{8}$$

where $\omega = \gamma B t$, $B = |\mathbf{B}|$, and $\gamma = \mu_B g_f/\hbar$ is the atomic gyromagnetic ratio. By fitting theses signals, we extract the vector field $\mathbf{B}$ and the FID transverse relaxation time $T_2 = 1/(\sigma\gamma\partial B/\partial z)$. An example measurement is shown in Fig. 7(b). For the data shown we find $B_x = 9.6 \pm 0.4$ mG, $B_y = 9.7 \pm 0.4$ mG, $B_z = 9.9 \pm 0.1$ mG and $T_2 = 745 \pm 45$ μs.

Noise scaling

To estimate the atomic noise contribution to the observed total variance $\mathcal{V} = \mathrm{Tr}(\Gamma)$ of the QND measurements we fit the polynomial $\mathcal{V}(N_A) = \mathcal{V}_0 + 2N_A + cN_A^2$ to the measured data, and calculate $\widetilde{\mathcal{V}}_p = \mathcal{V}_p - \mathcal{V}_0$, subtracting the read-out noise $\mathcal{V}_0$ from the measured total variances. The data and resulting fits are shown in Fig. 7(c). The fit to the first (second) measurement yields $\mathcal{V}_0 = 2.59 \pm 0.08 \times 10^6$ ($2.49 \pm 0.08 \times 10^6$) and $c = 4 \pm 2 \times 10^{-7}$ ($1 \pm 2 \times 10^{-7}$). We fit the polynomial $\mathcal{V}_{2|1}(N_A) = \mathcal{V}_0 + aN_A + cN_A^2$ to the measured conditional variance, giving $\mathcal{V}_0 = 9.2 \pm 0.8 \times 10^5$, $a = 0.9 \pm 3$ and $c = -4 \pm 2 \times 10^{-7}$, indicating the presence of some correlated technical noise in the detection system.